

Structure factors for the simplest solvable model of polydisperse colloidal fluids with surface adhesion

Domenico Gazzillo and Achille Giacometti

Istituto Nazionale di Fisica della Materia and

Facoltà di Scienze, Università di Venezia,

S. Marta DD 2137, I-30123 Venezia, Italy

(October 28, 2018)

Abstract

Closed analytical expressions for scattering intensity and other global structure factors are derived for a new solvable model of polydisperse sticky hard spheres. The starting point is the exact solution of the “mean spherical approximation” for hard core plus Yukawa potentials, in the limit of infinite amplitude and vanishing range of the attractive tail, with their product remaining constant. The choice of factorizable coupling (stickiness) parameters in the Yukawa term yields a simpler “dyadic structure” in the Fourier transform of the Baxter factor correlation function $q_{ij}(r)$, with a remarkable simplification in all structure functions with respect to previous works. The effect of size and stickiness polydispersity is analyzed and numerical results are presented for two particular versions of the model: i) when all polydisperse particles have a single, size-independent, stickiness parameter, and ii) when the stickiness parameters are proportional to the diameters. The existence of two different regimes for the average structure factor, respectively above and below a generalized Boyle temperature which depends on size polydispersity, is recognized and discussed. Because of its analyticity and simplicity, the model may be useful in the interpretation of small-angle scattering experimental data for polydisperse colloidal fluids of neutral particles with surface adhesion.

I. INTRODUCTION

A theoretical determination of scattering intensity and structure factors for fluids with a large number p of components is, in general, a difficult task. In particular, this is true when some kind of polydispersity is present, as occurs in colloidal or micellar solutions¹⁻³. Size polydispersity means that macroparticles of a same chemical species exhibit several different dimensions within a discrete or continuous set of possible values. Interaction polydispersity then denotes a similar, and usually correlated, dispersion of parameters (charges, etc.) defining the strength of interaction potentials. Even when all macroparticles belong to a unique chemical species, a polydisperse fluid must therefore be treated as a multi-component mixture, with very large p values (of order $10^1 \div 10^3$) or, in the infinite-component limit $p \rightarrow \infty$, with an idealized continuous distribution of some properties⁴.

In structural studies on polydisperse colloidal fluids, a key role can be played by the models for which the Ornstein-Zernike (OZ) integral equations of the liquid state⁵ admit analytical solutions leading to closed expressions of scattering functions for any finite p and even for $p \rightarrow \infty$. A sufficient condition for this is that the Fourier transforms $\hat{q}_{ij}(k)$ of the functions $q_{ij}(r)$, solutions of the Baxter factorized version of the OZ equations^{6,7}, have a peculiar mathematical form, which we refer to as *dyadic* structure⁸ and will be illustrated in Section II C. Using the dyadicity, the explicit inversion of a related $p \times p$ matrix $\hat{\mathbf{Q}}(k)$ is always possible for arbitrary p and closed analytical expressions for the “partial” structure factors $S_{ij}(k)$ ⁹ can be obtained. The scattering intensity and other “global” structure factors are then calculated as weighted sums of all partial structure factors.

Usually, the above sums are performed numerically by evaluating $p(p+1)/2$ independent contributions $S_{ij}(k)$ at each k ^{4,10-12}. This procedure becomes numerically demanding for large p , as required in polydisperse mixtures. On the other hand, we stress that the dyadicity property also enables an alternative route (followed in the present work) which avoids the explicit computation of individual $S_{ij}(k)$. The weighted sums can, in fact, be worked out analytically, by a procedure originally proposed by Vrij¹³ and referred to as

“Vrij’s summation” hereafter. The resulting closed analytical expressions of “global” scattering functions hold true for *any* number p of components, can be easily applied to polydisperse fluids even in the limit $p \rightarrow \infty$, and are particularly suitable to fit experimental scattering data. Vrij¹³ first obtained a closed expression for the scattering intensity of polydisperse hard spheres (HS) within the Percus-Yevick (PY) approximation. Gazzillo *et al.*⁸ derived similar formulas for polydisperse charged hard spheres (CHS), by using the corresponding analytical solution within the “mean spherical approximation” (MSA).

In the present paper we extend the approach previously exploited for polydisperse HS¹³ and CHS⁸ to polydisperse “sticky” hard spheres (SHS). This simple model adds to an interparticle hard core repulsion an infinitely strong attraction at contact, and can be applied to real colloidal fluids of neutral spherical particles with a van der Waals (or dispersion) force of attraction, working at very short distances.

Baxter¹⁴ proposed the one-component original version of this model, solved the OZ equation with the PY closure and found that such a system presents a liquid-gas phase transition. The adhesive contribution in Baxter’s Hamiltonian is defined by a particular limiting case of a square-well tail in which the depth goes to infinity as the width goes to zero, in such a way that the contribution to the second virial coefficient remains finite but not zero (Baxter limit). Stell¹⁵ found that SHS of equal diameter in the Baxter limit, when treated exactly rather than in the PY approximation, are not thermodynamically stable. Nevertheless, the PY solution for SHS as a useful colloidal model has received a continuously growing interest in the last two decades^{15,16}, partially because of its capability to exhibit a gas-liquid phase transition.

Perram and Smith¹⁷ and Barboy and Tenne¹⁸ extended Baxter’s work to p -component fluids, using the same kind of Hamiltonian and the PY approximation. Santos *et al.*¹⁹ developed a rational function approximation to go beyond the PY approximation and derived improved expressions for the radial distribution functions and structure factors of SHS mixtures.

Unfortunately, the PY analytical solution for mixtures requires the determination of

a set of unknown *density-dependent* parameters λ_{ij} , related, through $p(p + 1)/2$ coupled quadratic equations, to other parameters τ_{ij} which appear in the potentials as monotonically increasing functions of the temperature T and whose inverses measure the degree of adhesion (“stickiness”) of interacting spheres. In most cases the coefficients λ_{ij} for given τ_{ij} can only be found numerically, and this feature limits the applicability of the SHS-PY model to small p values. As a matter of fact the number of actual applications to polydisperse fluids is very limited. We are aware of a study by Robertus *et al.*²⁰ on small angle x-ray scattering from microemulsions, with polydispersity represented by $p = 9$ components, a work by Penders and Vrij²¹ on turbidity of silica particles, and an investigation by Duits *et al.*²² on small angle neutron scattering from sterically stabilized silica particles dispersed in benzene. To simplify the numerical determination of the set $\{\lambda_{ij}\}$, all these papers treat the special case of a single stickiness parameter, τ , independent of particle size.

In general, the SHS-PY solution for mixtures does not have the dyadic structure which allows the *analytic* inversion of $\widehat{\mathbf{Q}}(k)$ required to get closed expressions for structure factors of polydisperse systems. To recover the dyadicity and obtain an explicitly solvable model, Herrera and Blum²³ used the *ad hoc* assumption $\lambda_{ij} = \lambda_i \lambda_j$, in a study on polydisperse CHS with sticky interactions under a MSA/PY closure.

On the other hand, apart from Baxter’s original definition¹⁴, there exists a second version of the SHS model, proposed in the one-component case by Brey *et al.*²⁴ and Mier-y-Teran *et al.*²⁵. Here, the adhesive part of the potential is defined as the limit of a Yukawa tail when both amplitude and inverse range tend to infinity, with their ratio remaining constant. The analytic solution was obtained within the MSA closure²⁵, and Ginoza and Yasutomi²⁶ discussed its relationship to Baxter’s PY solution. Recently, Tutschka and Kahl²⁷ investigated the multi-component version of this second SHS model and presented MSA expressions of structure functions for both the discrete (finite p) and the continuous ($p \rightarrow \infty$) polydisperse case. These authors pointed out that the dyadic structure of the SHS-MSA solution can be ensured *a priori* by imposing from the outset a Berthelot-type rule⁵ on the coupling (stickiness) parameters γ_{ij} of the Yukawa tail, i.e. $\gamma_{ij} = (\gamma_{ii} \gamma_{jj})^{1/2}$.

Within the same framework of Yukawa-MSA models, the present paper has a threefold aim: i) we shall show that a new choice of Yukawa coupling parameters, Y_i , slightly different from Tutschka and Kahl's ones²⁷, can produce an even simpler solvable model of SHS, with a remarkable simplification of all analytical results; ii) we shall obtain closed analytical expressions for scattering intensity and other “global” structure factors of SHS by extending the formalism successfully employed for HS and CHS; iii) we shall present numerical applications not only in the case of equal stickiness for all particles, but also when a simple size-dependence of the stickiness parameters Y_i is assumed.

The interplay among stickiness attraction, size polydispersity, and hard core repulsion gives rise to a rather complex behaviour. Nonetheless we shall present a simple unified description of these results, hinging on the introduction of a generalized Boyle temperature.

The paper is organized as follows. In the next section the basic theory on structure factors, integral equations and dyadic matrices will be briefly recalled. The SHS model, its MSA solution under the assumption of factorizable coefficients, expressions for scattering intensity and other “global” structure factors will be given in Sec. III. Numerical results are included in Sec. IV, while the last section is devoted to a summary and some conclusive remarks.

II. BASIC FORMALISM

A. Structure factors and scattering intensity

All scattering functions of multicomponent or polydisperse fluids with spherically symmetric interparticle potentials can be expressed in terms of “partial” structure factors $S_{ij}(k)$, such as the Ashcroft-Langreth ones⁹

$$S_{ij}(k) = \delta_{ij} + H_{ij}(k) = \delta_{ij} + (\rho_i \rho_j)^{1/2} \tilde{h}_{ij}(k). \quad (1)$$

Here, k is the magnitude of the scattering vector, δ_{ij} the Kronecker delta, ρ_i the number density of species i , $\tilde{h}_{ij}(k)$ the three-dimensional Fourier transform of the total correlation

function, $h_{ij}(r) = g_{ij}(r) - 1$, with $g_{ij}(r)$ being the radial distribution function between two particles of species i and j at distance r .

The knowledge of the $S_{ij}(k)$ allows to calculate the scattering intensity as well as some “global” structure factors. The *coherent scattering intensity* $I(k)$ for a p -component fluid is given by^{1,13}

$$R(k) \equiv I(k)/V = \rho \sum_{i,j=1}^p (x_i x_j)^{1/2} F_i(k) F_j^*(k) S_{ij}(k), \quad (2)$$

where V is the volume, $\rho = \sum_m \rho_m$ the total number density, while $x_i = \rho_i/\rho$ and $F_i(k)$ denote the molar fraction and form factor of species i , respectively (the asterisk means complex conjugation). The *measurable average structure factor* is then defined from the Rayleigh ratio $R(k)$ as^{1,13}

$$S_M(k) = R(k) / [\rho P(k)]. \quad (3)$$

with $P(k) = \sum_{m=1}^p x_m |F_m(k)|^2$. As a third useful quantity, we consider the Bathia-Tornton *number-number structure factor*²⁸, which is related to number density fluctuations:

$$S_{NN}(k) = \sum_{i,j=1}^p (x_i x_j)^{1/2} S_{ij}(k). \quad (4)$$

The definition of other global structure factors may be found in Ref. 3. Clearly, $R(k)$, $S_M(k)$ and $S_{NN}(k)$ involve a unique kind of weighted sum, i.e.,

$$\sum_{i,j=1}^p w_i(k) w_j^*(k) S_{ij}(k), \quad (5)$$

with $w_i(k)$ being equal to $\rho_i^{1/2} F_i(k)$, $[x_i/P(k)]^{1/2} F_i(k)$, and $x_i^{1/2}$, respectively.

B. Integral equations in Baxter form

Integral equations of the liquid state theory represent a powerful theoretical tool to get the $h_{ij}(r)$ required to calculate the partial structure factors $S_{ij}(k)$. The Ornstein-Zernike (OZ) integral equations relate the $h_{ij}(r)$ functions to the simpler direct correlation functions $c_{ij}(r)$. For fluids with spherically symmetric interactions, these equations are^{5,29}

$$h_{ij}(r) = c_{ij}(r) + \sum_{m=1}^p \rho_m \int d\mathbf{r}' c_{im}(r') h_{mj}(|\mathbf{r} - \mathbf{r}'|) \quad (6)$$

and can be solved only when coupled with an approximate second relationship (a ‘‘closure’’) among $c_{ij}(r)$, $h_{ij}(r)$ and interparticle potential $u_{ij}(r)$ ^{5,29}.

By Fourier transformation, the OZ convolution equations become, in k -space,

$$[\mathbf{I} + \mathbf{H}(k)] [\mathbf{I} - \mathbf{C}(k)] = \mathbf{I}, \quad (7)$$

where $C_{ij}(k) \equiv (\rho_i \rho_j)^{1/2} \tilde{c}_{ij}(k)$ and $\tilde{c}_{ij}(k)$ is the Fourier transform of $c_{ij}(r)$. If $\mathbf{S}(k)$ denotes the symmetric matrix with elements $S_{ij}(k)$, then we get

$$\mathbf{S}(k) = \mathbf{I} + \mathbf{H}(k) = [\mathbf{I} - \mathbf{C}(k)]^{-1}, \quad (8)$$

with \mathbf{I} being the unit matrix of order p . The $S_{ij}(k)$ can therefore be expressed in terms not only of $\tilde{h}_{ij}(k)$, but also of $\tilde{c}_{ij}(k)$. However, in this paper we shall use a third representation of $S_{ij}(k)$ based upon the Baxter factor correlation functions $q_{ij}(r)$ ⁶. By means of a Wiener-Hopf factorization of $\mathbf{I} - \mathbf{C}(k)$, Baxter transformed the OZ equations for HS fluids into an equivalent, but easier to solve, form⁶. Later on these equations were extended by Hiroike to any spherically symmetric potentials, without using the Wiener-Hopf factorization⁷. Baxter factorization reads

$$\mathbf{I} - \mathbf{C}(k) = \widehat{\mathbf{Q}}^T(-k) \widehat{\mathbf{Q}}(k), \quad (9)$$

where $\widehat{\mathbf{Q}}(k)$ has the form

$$\widehat{\mathbf{Q}}(k) = \mathbf{I} - \tilde{\mathbf{Q}}(k) = \mathbf{I} - \int_{-\infty}^{+\infty} dr e^{ikr} \mathbf{Q}(r), \quad (10)$$

with $Q_{ij}(r) = 2\pi (\rho_i \rho_j)^{1/2} q_{ij}(r)$ ($\widehat{\mathbf{Q}}^T$ is the transpose of $\widehat{\mathbf{Q}}$). Note that $\widehat{Q}_{ij}(-k) = \widehat{Q}_{ij}^*(k)$. For fluids of particles with spherically symmetric interactions including HS repulsions (i.e., $u_{ij}(r) = +\infty$ when $r < \sigma_{ij} \equiv (\sigma_i + \sigma_j)/2$, with σ_i = hard sphere diameter of species i), the Baxter equations in r -space are

$$\left\{ \begin{array}{l} rc_{ij}(|r|) = -q'_{ij}(r) + 2\pi \sum_m \rho_m \int_{L_{mi}}^{\infty} dt q_{mi}(t) q'_{mj}(r+t), \\ rh_{ij}(|r|) = -q'_{ij}(r) + 2\pi \sum_m \rho_m \int_{L_{im}}^{\infty} dt q_{im}(t) (r-t) \\ \qquad \qquad \qquad \times h_{mj}(|r-t|), \end{array} \right. \quad (11)$$

where $r > L_{ij} \equiv (\sigma_i - \sigma_j)/2$ and the prime denotes differentiation with respect to r .

Using Eqs. (8) and (9), we get $\mathbf{S}(k) = \widehat{\mathbf{Q}}^{-1}(k) \left[\widehat{\mathbf{Q}}^{-1}(-k) \right]^T$ and the partial structure factors can be written as

$$S_{ij}(k) = \sum_m \widehat{Q}_{im}^{-1}(k) \widehat{Q}_{jm}^{-1}(-k) = \sum_m \widehat{Q}_{im}^{-1}(k) \left[\widehat{Q}_{jm}^{-1}(k) \right]^*. \quad (12)$$

On defining

$$s_m(k) = \sum_{i=1}^p w_i(k) \widehat{Q}_{im}^{-1}(k), \quad (13)$$

all the ‘‘global’’ structure functions can then be expressed as

$$\sum_{i,j=1}^p w_i(k) w_j^*(k) S_{ij}(k) = \sum_{m=1}^p s_m(k) s_m^*(k). \quad (14)$$

C. Dyadic matrices and Vrij’s summation

The main problem of these analytical calculations hinges on the inversion of the matrix $\widehat{\mathbf{Q}}(k) = \mathbf{I} - \widetilde{\mathbf{Q}}(k)$, which usually becomes a formidable task with increasing the number p of components. In a particular case, however, the inverse $\widehat{\mathbf{Q}}^{-1}(k)$ can be easily found for any size of the original matrix. This occurs when $\widehat{Q}_{ij}(k)$ is a *dyadic* (or Jacobi) matrix, i.e. when it has the peculiar mathematical structure

$$\widehat{Q}_{ij} = \delta_{ij} + \sum_{\mu=1}^n a_i^{(\mu)} b_j^{(\mu)} \quad (i, j = 1, \dots, p) \quad (15)$$

(the dependence on k was omitted for simplicity). We recall that a matrix $T_{ij} = a_i b_j$ formed by the direct product of two vectors is often referred to as a *dyad*, \mathbf{ab} , while a linear

combination of dyads $\sum_{\mu} \lambda_{\mu} \mathbf{a}^{(\mu)} \mathbf{b}^{(\mu)}$ is called a *dyadic*³⁰. Moreover, we shall refer to a sum of n dyads as a *n-dyadic*.

We caution the reader that, since $\widehat{Q}_{ij}(k) = \delta_{ij} - 2\pi (\rho_i \rho_j)^{1/2} \widehat{q}_{ij}(k)$, where $\widehat{q}_{ij}(k)$ is the unidimensional Fourier transform of $q_{ij}(r)$, Eq. (15) actually requires that $\widehat{q}_{ij}(k)$ is a n -dyadic matrix (of order p), but in the following we shall use the same terminology for $\widehat{Q}_{ij}(k)$ as well. The dyadicity is actually present in some solvable models of fluid mixtures: $\widehat{q}_{ij}(k)$ is 2-dyadic in the PY solution for neutral HS^{4,13}, and 3-dyadic in the MSA solution for CHS³¹.

The dyadic matrices have some special properties, which have already been partially discussed in Ref. 8. Here we recall the main points along with new additional features. Let us associate to the matrix of order p of Eq. (15), $\widehat{\mathbf{Q}} = \mathbf{I} + \sum_{\mu=1}^n \mathbf{a}^{(\mu)} \mathbf{b}^{(\mu)}$, a matrix \mathbf{D}_Q of order n with elements

$$d_{\alpha\beta} = \delta_{\alpha\beta} + \mathbf{a}^{(\alpha)} \cdot \mathbf{b}^{(\beta)} \quad (\alpha, \beta = 1, \dots, n), \quad (16)$$

where the dot denotes the usual scalar product of vectors, i.e. $\mathbf{a}^{(\alpha)} \cdot \mathbf{b}^{(\beta)} = \sum_{m=1}^p a_m^{(\alpha)} b_m^{(\beta)}$. A first property is that any n -dyadic matrix $\widehat{\mathbf{Q}}$ of order p has always rank n , irrespective of p . Moreover, its determinant $|\widehat{\mathbf{Q}}|$, which is of order p , turns out to be equal to the determinant $D_Q \equiv |\mathbf{D}_Q|$ of order n (with $n \ll p$ in multi-component fluids). A second property yields the explicit form of the elements of the inverse matrix $\widehat{\mathbf{Q}}^{-1}$, as

$$\widehat{Q}_{ij}^{-1} = \delta_{ij} - \frac{1}{D_Q} \sum_{\alpha=1}^n \sum_{\beta=1}^n a_i^{(\alpha)} b_j^{(\beta)} |\mathbf{D}_Q|^{\alpha\beta}, \quad (17)$$

where $|\mathbf{D}_Q|^{\alpha\beta}$ is the cofactor of the (α, β) th element in \mathbf{D}_Q and the double sum contains n^2 determinants of order n . Clearly, this expression could also be rewritten as a sum of only n determinants, i.e., $\widehat{Q}_{ij}^{-1} = \delta_{ij} - \sum_{\alpha=1}^n a_i^{(\alpha)} \widehat{D}_j^{(\alpha)} / D_Q$, where $\widehat{D}_j^{(\alpha)} \equiv \sum_{\beta=1}^n b_j^{(\beta)} |\mathbf{D}_Q|^{\alpha\beta}$ is the determinant obtained from D_Q by replacing the α -th *row* with $b_j^{(1)}, \dots, b_j^{(n)}$. Alternatively, one could write $\widehat{Q}_{ij}^{-1} = \delta_{ij} - \sum_{\beta=1}^n D_i^{(\beta)} b_j^{(\beta)} / D_Q$, with $D_i^{(\beta)} \equiv \sum_{\alpha=1}^n a_i^{(\alpha)} |\mathbf{D}_Q|^{\alpha\beta}$ being obtained from D_Q by replacing the β -th *column* with $a_i^{(1)}, \dots, a_i^{(n)}$ (Cramer rule).

All above expressions reflect the remarkable fact that $\widehat{\mathbf{Q}}^{-1}$ is a n -dyadic matrix as well, and it is indeed this property enabling a successful outcome of Vrij's summation for "global"

structure functions. Our starting point is a reformulation of Eq. (17) in terms of a determinant of order $n + 1$:

$$\widehat{Q}_{ij}^{-1} = \frac{1}{D_Q} \begin{vmatrix} \delta_{ij} & b_j^{(1)} & b_j^{(2)} & \cdots & b_j^{(n)} \\ a_i^{(1)} & 1 + \mathbf{a}^{(1)} \cdot \mathbf{b}^{(1)} & \mathbf{a}^{(1)} \cdot \mathbf{b}^{(2)} & \cdots & \mathbf{a}^{(1)} \cdot \mathbf{b}^{(n)} \\ a_i^{(2)} & \mathbf{a}^{(2)} \cdot \mathbf{b}^{(1)} & 1 + \mathbf{a}^{(2)} \cdot \mathbf{b}^{(2)} & \cdots & \mathbf{a}^{(2)} \cdot \mathbf{b}^{(n)} \\ \vdots & \vdots & \vdots & \vdots & \vdots \\ a_i^{(n)} & \mathbf{a}^{(n)} \cdot \mathbf{b}^{(1)} & \mathbf{a}^{(n)} \cdot \mathbf{b}^{(2)} & \cdots & 1 + \mathbf{a}^{(n)} \cdot \mathbf{b}^{(n)} \end{vmatrix}, \quad (18)$$

where \mathbf{D}_Q is included as a submatrix. From Eqs. (13) and (18), one then gets

$$s_m = \frac{1}{D_Q} \begin{vmatrix} w_m & b_m^{(1)} & b_m^{(2)} & \cdots & b_m^{(n)} \\ \mathbf{w} \cdot \mathbf{a}^{(1)} & d_{11} & d_{12} & \cdots & d_{1n} \\ \mathbf{w} \cdot \mathbf{a}^{(2)} & d_{21} & d_{22} & \cdots & d_{2n} \\ \vdots & \vdots & \vdots & \vdots & \vdots \\ \mathbf{w} \cdot \mathbf{a}^{(n)} & d_{n1} & d_{n2} & \cdots & d_{nn} \end{vmatrix}. \quad (19)$$

To perform the sum over m required in Eq. (14), we expand this determinant along the first row to get

$$s_m = w_m + \sum_{\alpha=1}^n b_m^{(\alpha)} C_\alpha, \quad (20)$$

where $C_\alpha \equiv T_\alpha/D_Q$ and T_α ($\alpha = 0, 1, \dots, n$) is the cofactor of the element $(1, \alpha + 1)$ th in the determinant of Eq. (19). Clearly, $T_0 = D_Q$. Using Eqs. (14) and (20), the searched final result is

$$\sum_{i,j=1}^p w_i w_j^* S_{ij} = \mathbf{w} \cdot \mathbf{w}^* + 2 \sum_{\alpha=1}^n \text{Re} [\mathbf{w}^* \cdot \mathbf{b}^{(\alpha)} C_\alpha] + \sum_{\alpha=1}^n \sum_{\beta=1}^n \mathbf{b}^{(\alpha)} \cdot \mathbf{b}^{(\beta)*} C_\alpha C_\beta^*, \quad (21)$$

where $\text{Re}[\dots]$ denotes the real part of a complex number. Vrij¹³ first performed a similar computation and derived a closed expression for the scattering intensity of HS mixtures. Our expression generalizes Vrij's one as well as that of Ref. 8 for the scattering intensity of CHS. It is simpler and more compact and can be used to calculate any "global" structure function, for mixtures with *any* number p of components. It involves a sum of only $(n + 1)^2$

terms, and depends on p through some averages represented by scalar products of vectors. Only the number of terms contained in these averages increases with increasing p , and hence the application to polydisperse mixtures is straightforward.

III. THE MODEL

A. Sticky hard spheres as a limit of Yukawa particles

A fluid of SHS can be derived from particles interacting via HS plus Yukawa (HSY) attractive potentials, i.e.

$$-\beta u_{ij}(r) = \begin{cases} +\infty, & 0 < r < \sigma_{ij} \\ \beta A_{ij} e^{-\mu(r-\sigma_{ij})}/r, & r > \sigma_{ij} \end{cases}, \quad (22)$$

in the limit $\mu \rightarrow +\infty$ with $\beta A_{ij} = \mu K_{ij}$ and K_{ij} independent of μ . Here, $\beta = (k_B T)^{-1}$, where k_B is the Boltzmann constant, and all A_{ij} are positive, with $A_{ji} = A_{ij}$ and $K_{ji} = K_{ij}$, as required by the symmetry condition $u_{ji}(r) = u_{ij}(r)$. This approach is convenient, since the Baxter equations for HSY mixtures have been solved analytically³², for any finite μ , within the MSA closure, which adds to the exact hard core condition, $h_{ij}(r) = -1$ for $r < \sigma_{ij}$, the approximate relationship $c_{ij}(r) = -\beta u_{ij}(r)$ for $r > \sigma_{ij}$. The solution is

$$q_{ij}(r) = \begin{cases} 0, & r < L_{ij} \\ \frac{1}{2}a_i(r - \sigma_{ij})^2 + (b_i + a_i\sigma_{ij})(r - \sigma_{ij}) + C_{ij} [e^{-\mu(r-\sigma_{ij})} - 1] \\ \quad + D_{ij}e^{-\mu(r-\sigma_{ij})}, & L_{ij} < r < \sigma_{ij} \\ D_{ij}e^{-\mu(r-\sigma_{ij})}, & r > \sigma_{ij} \end{cases} \quad (23)$$

where the coefficients are determined by a complicate set of equations³². From these, however, it can be shown that, as $\mu \rightarrow +\infty$, then $C_{ij} \rightarrow -D_{ij}$ and $D_{ij} \rightarrow \beta A_{ij}/\mu = K_{ij}$. The MSA solution for SHS is therefore

$$q_{ij}(r) = \begin{cases} \frac{1}{2}a_i(r - \sigma_{ij})^2 + (b_i + a_i\sigma_{ij})(r - \sigma_{ij}) + K_{ij}, & L_{ij} \leq r \leq \sigma_{ij} \\ 0, & \text{elsewhere} \end{cases} \quad (24)$$

$$a_i = \frac{1}{\Delta} + \frac{3\xi_2\sigma_i}{\Delta^2} - \frac{12\zeta_i}{\Delta}, \quad b_i = \left(\frac{1}{\Delta} - a_i \right) \frac{\sigma_i}{2}, \quad (25)$$

$$\xi_m = \frac{\pi}{6} \sum_{i=1}^p \rho_i \sigma_i^m, \quad \zeta_i = \frac{\pi}{6} \sum_{j=1}^p \rho_j \sigma_j K_{ij}, \quad \Delta = 1 - \xi_3. \quad (26)$$

To calculate $\widehat{Q}_{ij}^{-1}(k)$, we need the unidimensional Fourier transform $\widehat{q}_{ij}(k)$, i.e.

$$\begin{aligned} \widehat{q}_{ij}(k) = -e^{iX_i} \left\{ \left(1 + \frac{3\xi_2\sigma_i}{\Delta} - 12\zeta_i \right) \frac{1}{4\Delta} \sigma_j^3 \frac{j_1(X_j)}{X_j} \right. \\ \left. + \frac{1}{4\Delta} \sigma_i \sigma_j^2 [j_0(X_j) - ij_1(X_j)] - K_{ij} \sigma_j j_0(X_j) \right\}, \end{aligned} \quad (27)$$

where $X_m \equiv k\sigma_m/2$, $j_0(x) = \sin x/x$ and $j_1(x) = (\sin x - x \cos x)/x^2$ are spherical Bessel functions, and i - when it is not a subscript - is the imaginary unit.

B. Factorizable coefficients

In general $\widehat{q}_{ij}(k)$, as defined in Eq. (27), does not have the required dyadic structure, due to the presence of K_{ij} in the last term. To overcome this difficulty, Tutschka and Kahl²⁷ proposed the following *Ansatz*:

$$K_{ij} = \gamma_{ij} \sigma_{ij}^2, \quad \text{with} \quad \gamma_{ij} = (\gamma_{ii} \gamma_{jj})^{1/2} \quad (\text{Berthelot-rule}), \quad (28)$$

which yields $K_{ij} = \gamma_{ii}^{1/2} \gamma_{jj}^{1/2} (\sigma_i^2 + 2\sigma_i \sigma_j + \sigma_j^2)/4$. Consequently, the last term of Eq. (27) splits into three independent contributions, and $\widehat{q}_{ij}(k)$ turns out to be 5-dyadic, in spite of the fact that in the HS limit (no adhesion) it is only 2-dyadic.

We first note that a great simplification occurs with the factorization

$$K_{ij} = Y_i Y_j \quad (29)$$

(all $Y_m \geq 0$). In this case, the last term of Eq. (27) generates only one contribution, and $\widehat{q}_{ij}(k)$ becomes simply 3-dyadic and, in a particular case to be discussed later on, even 2-dyadic. The K_{ij} defined by Eq. (29) satisfy the Berthelot-rule, i.e. $K_{ij} = (K_{ii} K_{jj})^{1/2}$. Note that the stickiness parameters γ_{mm} are dimensionless²⁷, while the Y_m are lengths.

Factorizable adhesive parameters have already been considered by Yasutomi and Ginoza³³ and Herrera *et al.*³⁴ in studies on adhesive-HSY fluids, although no expressions for structure functions were given. Since in those papers $K_{ij} = GG_iG_j$, the relationship with our coefficients is simply given by $Y_m = G^{1/2}G_m$.

Using Eq. (29), we get $\zeta_i = \xi_2^Y Y_i$ with $\xi_2^Y \equiv (\pi/6) \sum_{j=1}^p \rho_j \sigma_j Y_j$ (dimensionally analogous to ξ_2), and therefore

$$\begin{aligned} \widehat{Q}_{ij}(k) &= \delta_{ij} - 2\pi (\rho_i \rho_j)^{1/2} \widehat{q}_{ij}(k) \\ &= \delta_{ij} + \rho_i^{1/2} e^{iX_i} \left\{ \left(1 + \frac{3\xi_2 \sigma_i}{\Delta} - i \frac{k \sigma_i}{2} - 12\xi_2^Y Y_i \right) \frac{\pi}{2\Delta} \sigma_j^3 \frac{j_1(X_j)}{X_j} \right. \\ &\quad \left. + \frac{\pi}{2\Delta} \sigma_i \sigma_j^2 j_0(X_j) - 2\pi Y_i Y_j \sigma_j j_0(X_j) \right\} \rho_j^{1/2}, \end{aligned} \quad (30)$$

which has the required dyadic structure $\widehat{Q}_{ij} = \delta_{ij} + \sum_{\mu=1}^n a_i^{(\mu)} b_j^{(\mu)}$. We emphasize that the decomposition into $a_i^{(\mu)}$ and $b_j^{(\mu)}$ is not unique. Our choice allows an easy comparison with the corresponding results for polydisperse HS¹³ and CHS⁸. After defining

$$\begin{aligned} \alpha_m(k) &= \frac{\pi}{2\Delta} \sigma_m^3 \frac{j_1(X_m)}{X_m}, \\ \beta_m^{(0)}(k) &= \frac{\pi}{2\Delta} \sigma_m^2 j_0(X_m), \quad \beta_m(k) = \beta_m^{(0)}(k) + \left(\frac{3\xi_2}{\Delta} - i \frac{k}{2} \right) \alpha_m(k), \\ \delta_m^{(0)}(k) &= -2\pi \sigma_m Y_m j_0(X_m), \quad \delta_m(k) = \delta_m^{(0)}(k) - 12\xi_2^Y \alpha_m(k), \end{aligned} \quad (31)$$

$\widehat{Q}_{ij}(k)$ may be rewritten as

$$\widehat{Q}_{ij}(k) = \delta_{ij} + \rho_i^{1/2} e^{iX_i} [\alpha_j(k) + \sigma_i \beta_j(k) + Y_i \delta_j(k)] \rho_j^{1/2}, \quad (32)$$

and the corresponding decomposition is

$$\begin{aligned} a_i^{(1)} &= \rho_i^{1/2} e^{iX_i}, & b_j^{(1)} &= \rho_j^{1/2} \alpha_j, \\ a_i^{(2)} &= \rho_i^{1/2} e^{iX_i} \sigma_i, & b_j^{(2)} &= \rho_j^{1/2} \beta_j, \\ a_i^{(3)} &= \rho_i^{1/2} e^{iX_i} Y_i, & b_j^{(3)} &= \rho_j^{1/2} \delta_j. \end{aligned} \quad (33)$$

If we are interested in the scattering intensity, then Eq. (19) with $w_m = \rho_m^{1/2} F_m$ yields

$$s_m = \frac{\rho_m^{1/2}}{D_Q} \begin{vmatrix} F_m & \alpha_m & \beta_m & \delta_m \\ \{F\} & 1 + \{\alpha\} & \{\beta\} & \{\delta\} \\ \{\sigma F\} & \{\sigma\alpha\} & 1 + \{\sigma\beta\} & \{\sigma\delta\} \\ \{YF\} & \{Y\alpha\} & \{Y\beta\} & 1 + \{Y\delta\} \end{vmatrix} \quad (34)$$

where D_Q coincides with the cofactor of the (1,1)th element in the 4×4 determinant, and

$$\{fg\} \equiv \sum_{m=1}^p \rho_m e^{iX_m} f_m g_m = \rho \langle e^{iX} fg \rangle, \quad \langle f \rangle \equiv \sum_{m=1}^p x_m f_m. \quad (35)$$

Here and in the following, angular brackets $\langle \dots \rangle$ denote compositional averages over the distribution of particles (this notation differs from that of Ref. 8, which also contains misprints corrected in Refs. 35,36).

With the chosen decomposition of $\widehat{Q}_{ij}(k)$ the stickiness contributions are confined in the last row and the last column of the determinant of Eq. (34). When adhesion is turned off, all these elements vanish apart from their diagonal term, and the 4×4 determinant essentially reduces to the 3×3 HS one. For numerical computation, it is convenient, following Ref. 8, to simplify s_m by using elementary transformations which do not alter the value of the determinant. If we add to the third column the second one multiplied by $-(3\xi_2/\Delta - ik/2)$ and to the fourth column the second one multiplied by $12\xi_2^Y$, then s_m becomes

$$s_m = \frac{\rho_m^{1/2}}{D_Q} \begin{vmatrix} F_m & \alpha_m & \beta_m^{(0)} & \delta_m^{(0)} \\ \{F\} & 1 + \{\alpha\} & \{\beta^{(0)}\} - 3\xi_2/\Delta + ik/2 & \{\delta^{(0)}\} + 12\xi_2^Y \\ \{\sigma F\} & \{\sigma\alpha\} & 1 + \{\sigma\beta^{(0)}\} & \{\sigma\delta^{(0)}\} \\ \{YF\} & \{Y\alpha\} & \{Y\beta^{(0)}\} & 1 + \{Y\delta^{(0)}\} \end{vmatrix}, \quad (36)$$

where D_Q has been changed accordingly. Expanding the 4×4 determinant along the first line and inserting it into Eq. (14), the final result for the scattering intensity of SHS is

$$\begin{aligned} R(k)/\rho &= \langle F^2 \rangle + \langle \alpha^2 \rangle |C_1|^2 + \langle \beta^{(0)2} \rangle |C_2|^2 + \langle \delta^{(0)2} \rangle |C_3|^2 \\ &+ 2 \operatorname{Re} [\langle F\alpha \rangle C_1 + \langle F\beta^{(0)} \rangle C_2 + \langle F\delta^{(0)} \rangle C_3 \\ &+ \langle \alpha\beta^{(0)} \rangle C_1 C_2^* + \langle \alpha\delta^{(0)} \rangle C_1 C_3^* + \langle \beta^{(0)}\delta^{(0)} \rangle C_2 C_3^*], \end{aligned} \quad (37)$$

where form factors have been assumed to be real quantities, as is indeed the case for spherical homogeneous scattering cores. On the r.h.s. all k arguments have been omitted for simplicity, and the $C_\nu(k)$ have already been defined with reference to Eq. (20).

The expression for the average structure factor $S_M(k)$ is then obtained after division of the Rayleigh ratio $R(k)$ by $\rho P(k) = \rho \langle F^2(k) \rangle$. Moreover, the Bathia-Thornton number-number structure factor $S_{NN}(k)$ can easily be derived by setting all $F_m = 1$ everywhere into the expression of $R(k)/\rho$, with the result

$$\begin{aligned}
S_{NN}(k) = & 1 + \rho \{ \langle \alpha^2 \rangle |\mathcal{C}_1|^2 + \langle \beta^{(0)2} \rangle |\mathcal{C}_2|^2 + \langle \delta^{(0)2} \rangle |\mathcal{C}_3|^2 \\
& + 2 \operatorname{Re} [\langle \alpha \rangle \mathcal{C}_1 + \langle \beta^{(0)} \rangle \mathcal{C}_2 + \langle \delta^{(0)} \rangle \mathcal{C}_3 \\
& + \langle \alpha \beta^{(0)} \rangle \mathcal{C}_1 \mathcal{C}_2^* + \langle \alpha \delta^{(0)} \rangle \mathcal{C}_1 \mathcal{C}_3^* + \langle \beta^{(0)} \delta^{(0)} \rangle \mathcal{C}_2 \mathcal{C}_3^*] \},
\end{aligned} \tag{38}$$

where the \mathcal{C}_ν are the analogues of the C_ν appearing in $R(k)$.

IV. RESULTS FOR POLYDISPERSE FLUIDS

A. Size distribution

For SHS fluids containing only one chemical species, size polydispersity simply means the presence of a multiplicity of possible diameters. In a “discrete” representation of polydispersity the number p of different diameters is very large but finite, and x_i is the fraction N_i/N of particles having diameter σ_i . On the other hand, a theoretical representation with infinitely many components ($p \rightarrow \infty$) and “continuously” distributed diameters is also possible and often used.

Although all formulas of previous Sections refer to a finite number p of components, the polydisperse continuous limit of such expressions can immediately be inferred by the *replacement rules* $x_\alpha \rightarrow dx = f(\sigma)d\sigma$ and $\sum_\alpha x_\alpha \dots \rightarrow \int d\sigma f(\sigma) \dots$, where $f(\sigma)d\sigma$ is the fraction dN/N of particles with diameter in the interval $(\sigma, \sigma + d\sigma)$. As *molar fraction density function* $f(\sigma)$ we choose the Schulz distribution^{37,38}

$$f(\sigma) = \frac{a}{\Gamma(a) \langle \sigma \rangle} \left(a \frac{\sigma}{\langle \sigma \rangle} \right)^{a-1} \exp \left(-a \frac{\sigma}{\langle \sigma \rangle} \right) \quad (a > 1), \quad (39)$$

where Γ is the gamma function³⁹, $\langle \sigma \rangle$ the average diameter, $a = 1/s_\sigma^2$, and $s_\sigma = [\langle \sigma^2 \rangle - \langle \sigma \rangle^2]^{1/2} / \langle \sigma \rangle$ measures the degree of size polydispersity. In the monodisperse limit, $s_\sigma = 0$, the distribution becomes a Dirac delta function centered at $\langle \sigma \rangle$. The Schulz function allows an easy analytic evaluation of some averages $\int d\sigma f(\sigma) \dots$, such as the moments $\langle \sigma^m \rangle$, which obey a simple relation for $m \geq 1$, i.e.

$$\langle \sigma^m \rangle = [1 + (m-1)s_\sigma^2] \langle \sigma \rangle \langle \sigma^{m-1} \rangle = \langle \sigma \rangle^m \prod_{j=1}^{m-1} M_j, \quad (40)$$

with $M_j \equiv 1 + js_\sigma^2$.

In most cases, however, analytical integration is hardly feasible, and numerical integration brings back to discrete expressions with large p , of order $10^2 - 10^3$. In practice, the “discrete” representation of polydispersity is the most convenient for numerical purposes, and all formulas of the previous Sections can be employed by assuming $x_\alpha = f(\sigma_\alpha) \Delta\sigma$, where $\Delta\sigma$ is the grid size of numerical integration.

For fluids with Schulz-distributed diameters the packing fraction, $\eta \equiv \xi_3 = (\pi/6)\rho \langle \sigma^3 \rangle$, can be written as $\eta = \eta_{\text{mono}} (1 + s_\sigma^2) (1 + 2s_\sigma^2)$, with $\eta_{\text{mono}} = (\pi/6)\rho \langle \sigma \rangle^3$.

B. Stickiness distribution

On a dimensional basis, the parameters Y_i must be lengths. Moreover, $K_{ij} = Y_i Y_j$ must be proportional to $\beta = (k_B T)^{-1}$. If we assume, for simplicity, that stickiness polydispersity and size polydispersity are fully correlated, then the most natural choice for Y_i is

$$Y_i = \gamma_0 \sigma_i, \quad (41)$$

with the dimensionless proportionality factor

$$\gamma_0 = \left(\frac{\varepsilon_0}{k_B T} \right)^{1/2} = \frac{Y_{\langle \sigma \rangle}}{\langle \sigma \rangle}, \quad (42)$$

where ε_0 denotes an energy and $Y_{\langle\sigma\rangle}$ is the stickiness parameter of particles with diameter $\langle\sigma\rangle$. This implies that

$$K_{ij} = \gamma_0^2 \sigma_i \sigma_j = \frac{\varepsilon_0}{k_B T} \sigma_i \sigma_j = \frac{1}{T^*} \sigma_i \sigma_j, \quad (43)$$

where we have also introduced a reduced temperature $T^* = (k_B T / \varepsilon_0) \equiv 1 / \gamma_0^2$.

The model of Eq. (41) will be compared with the one of SHS polydisperse in size but not in stickiness (on the analogy of Refs. 20 and 21). In this simpler case all particles have the same $Y_i = Y_{\langle\sigma\rangle} = \gamma_0 \langle\sigma\rangle$, and the degree of stickiness polydispersity s_Y , defined similarly to s_σ , vanishes.

Both these models may be regarded as particular cases (for $\alpha = 0$ and $\alpha = 1$) of a more general size-dependence given by

$$Y_i = Y_{\langle\sigma\rangle} \left(\frac{\sigma_i}{\langle\sigma\rangle} \right)^\alpha = \gamma_0 \frac{\sigma_i^\alpha}{\langle\sigma\rangle^{\alpha-1}}, \quad (44)$$

with $\alpha \geq 0$. We have examined this generalization for $\alpha = 2$ and $\alpha = 3$, but for the purposes of the present paper we restrict our analysis only to the cases $\alpha = 0$ and $\alpha = 1$.

The choice $Y_i = \gamma_0 \sigma_i$ has very interesting properties. First, the corresponding distribution of Y -values, related to the size distribution f_σ as $f_Y \equiv dN/dY = f_\sigma d\sigma/dY$, is a Schulz function as well, with $\langle Y \rangle = Y_{\langle\sigma\rangle}$ and $s_Y = s_\sigma$. A second more important fact is that only in this special case $\widehat{Q}_{ij}(k)$, in general 3-dyadic for SHS, becomes simply 2-dyadic, i.e.

$$\widehat{Q}_{ij}(k) = \delta_{ij} + \rho_i^{1/2} e^{iX_i} \left\{ A_i(k) \alpha_j(k) + G_0 \sigma_i \beta_j^{(0)}(k) \right\} \rho_j^{1/2}, \quad (45)$$

with

$$A_i(k) = 1 + \left(\frac{3\xi_2 G_0}{\Delta} - i \frac{k}{2} \right) \sigma_i,$$

$$G_0 \equiv 1 - 4\gamma_0^2 \Delta = 1 - \frac{4\varepsilon_0}{k_B T} \left[1 - \eta_{\text{mono}} (1 + s_\sigma^2) (1 + 2s_\sigma^2) \right] \quad (46)$$

(now $\xi_2^Y = \gamma_0 \xi_2$). It is remarkable that this expression for $\widehat{Q}_{ij}(k)$ differs from the HS one only for the presence of G_0 ($G_0 = 1$ for HS). Now the natural dyadic decomposition becomes

$$\begin{aligned}
a_i^{(1)} &= \rho_i^{1/2} e^{iX_i} A_i, & b_j^{(1)} &= \rho_j^{1/2} \alpha_j, \\
a_i^{(2)} &= \rho_i^{1/2} e^{iX_i} G_0 \sigma_i, & b_j^{(2)} &= \rho_j^{1/2} \beta_j^{(0)},
\end{aligned}
\tag{47}$$

while the 4×4 determinant appearing in Eq. (34) reduces to a 3×3 one, with a consequent simplification of the formulas for $R(k)/\rho$, $S_M(k)$ and $S_{NN}(k)$ (all terms depending on subscript 3 vanish in Eqs. (37) and (38)).

C. Numerical results

Because of its importance in the analysis of experimental scattering data, we have focused on the measurable average structure factor $S_M(k)$. The scattering cores inside the particles have been assumed to be spherical and homogeneous, with form factors $F_m = V_m^{\text{scatt}} \Delta n_m 3j_1(X_m^{\text{scatt}})/X_m^{\text{scatt}}$, where $X_m^{\text{scatt}} = k\sigma_m^{\text{scatt}}/2$, $\sigma_m^{\text{scatt}} \leq \sigma_m$ is the diameter of a scattering core of species m , $V_m^{\text{scatt}} = (\pi/6)(\sigma_m^{\text{scatt}})^3$ its volume, and Δn_m its scattering contrast with respect to the solvent. For mixtures with several components belonging to only one chemical species, as in the present paper, Δn_m is the same for all particles. For simplicity, we have taken $\sigma_m^{\text{scatt}} = \sigma_m$.

The polydisperse SHS model depends on the following parameters: the packing fraction η , the strength γ_0 of the adhesive interaction, the average diameter $\langle \sigma \rangle$, and the two degrees of polydispersity s_σ and s_Y . In all numerical calculations we have adopted dimensionless variables, with lengths expressed in units of $\langle \sigma \rangle$. To understand the influence of each parameter on $S_M(k)$, it is instructive to first recall the behaviour of a sequence of simpler systems, starting from monodisperse hard spheres and adding in the first two cases either surface attraction or size polydispersity.

1. Monodisperse HS and SHS

In pure fluids all particles are equal ($s_\sigma = 0 = s_Y$), $\eta = \eta_{\text{mono}}$, and $S_M(k) = S_{\text{mono}}(k)$ with no form factor involved. Figures 1 and 2 depict the dependence of $S_{\text{mono}}(k)$ on the

parameters (η, γ_0) . Fig. 1 illustrates the evolution of $S_{\text{mono}}(k)$, as η increases from low values up to the freezing one, in the well known case of monodisperse HS of diameter σ without stickiness ($\gamma_0 = 0$). Here we have exploited the PY solution⁵, which, for HS, coincides with the MSA one. In Fig. 2 the dependence of $S_{\text{mono}}(k)$ on η is displayed for monodisperse SHS, at two fixed γ_0 values, i.e. 0.5 and 0.7, corresponding to $\gamma_0^2 = \varepsilon_0 / (k_B T) = 0.25$ and 0.49, or to $T^* = 4$ and 2.04 (γ_0 and T^* have been defined in Eqs. (42) and (43), respectively).

In all these cases (Figs. 1, 2a and 2b), as η increases at fixed γ_0 , the first peak height and amplitudes of all subsequent oscillations increase, but the behaviour near the origin depends on γ_0 , as will be discussed in more detail shortly.

On the other hand, the effect of increasing γ_0 (i.e. increasing the adhesive attraction or decreasing T) at fixed η can be seen by comparing, for instance, the solid curves ($\eta = 0.2$) of Figs. 1 and 2. As γ_0 increases, the first peak and subsequent maxima are shifted to larger k values, and their amplitudes change as well. However, the most significant effect on $S_{\text{mono}}(k)$ occurs near the origin. Here, $S_{\text{mono}}(0)$ substantially increases and becomes the global maximum at large γ_0 . This behaviour can be understood from the explicit expression of $S_{\text{mono}}(0)$, which reads

$$\begin{aligned} S_{\text{mono}}(0) &= \left[\widehat{Q}_{\text{mono}}(0) \right]^{-2} = \frac{(1 - \eta)^4}{[1 + 2\eta - 12\gamma_0^2 \eta (1 - \eta)]^2} \\ &= K_T / K_T^{\text{id}} = \rho k_B T K_T. \end{aligned} \quad (48)$$

Since $S_{\text{mono}}(0)$ is related to the isothermal osmotic compressibility K_T and to the density fluctuations⁴⁰, its drastic increase signals the approach to a gas-liquid phase transition. The critical point can be obtained from the spinodal line, defined by $S_{\text{mono}}^{-1}(0) = 0$, and the critical parameters turn out to be: $\eta_c = (\sqrt{3} - 1) / 2 \simeq 0.37$ and $\gamma_{0c}^2 = (\sqrt{3} + 2) / 6 \simeq 0.62$ ²⁴ (corresponding to $\gamma_{0c} \simeq 0.79$, or to the reduced *critical temperature* $T_c^* \simeq 1.61$).

The combined influence of η and γ_0 can be observed going back to Fig. 2. On defining the *Boyle temperature* T_B^* as the one where the attractive and repulsive forces balance each other in such a way that the second virial coefficient B_2 vanishes²¹, we note that the temperatures corresponding to $\gamma_0 = 0.5$ and 0.7 lie, respectively, above and below T_B^* (but in both cases

above T_c^*). In fact, for this monodisperse model it is easy to see, from the low-density expansion of $S_{\text{mono}}(0) = 1 + \rho \tilde{h}(0) \simeq 1 - 2B_2\rho + \mathcal{O}(\rho^2)$, that $B_2 = 4V_{\text{HS}}(1 - 3\gamma_0^2) = 4V_{\text{HS}}(1 - 3/T^*)$ with $V_{\text{HS}} = (\pi/6)\sigma^3$, and therefore $T_B^* = 3$ ($\gamma_{0B}^2 = 1/3$ or $\gamma_{0B} \simeq 0.58$). Fig. 2 suggests the existence of two different “regimes” for $S_{\text{mono}}(k)$ above and below the Boyle temperature, respectively. When $T^* > T_B^*$ or, equivalently, $\gamma_0 < \gamma_{0B}$ (“weak-attraction regime”, as in Fig. 2a) the fluid behaves like pure HS without stickiness. Here repulsive forces are dominant, $B_2 > 0$, and compressibility and density fluctuations, along with the whole $S_{\text{mono}}(k)$ near the origin, decrease with increasing η . When $T_c^* < T^* < T_B^*$ or, equivalently, $\gamma_{0B} < \gamma_0 < \gamma_{0c}$ (“strong-attraction regime”), one finds $B_2 < 0$, while the balance between attractive and repulsive forces becomes more complex. In this case $S_{\text{mono}}(k)$ near the origin has a non-monotonic dependence on η , as in Fig. 2b. Here, compressibility and density fluctuations first increase with η , in agreement with the low-density expansion of $S_{\text{mono}}(0)$. Then, an inversion occurs at $\eta_0 = (6 - 2T^*)/(6 + T^*)$ ($\simeq 0.24$ when $T^* = 2.04$) and afterwards $S_{\text{mono}}(0)$ decreases. In other words, below T_B^* attractive forces seem to be dominant at low packing fraction, whereas repulsion again prevails at higher η .

2. Polydisperse HS without stickiness

Fig. 3 refers to polydisperse HS without surface adhesion ($\gamma_0 = 0$). Size polydispersities $s_\sigma = 0.1, 0.3$ have been employed here and in the following, since values in this range are rather common in experimental data from colloidal fluids. The two Schulz distributions have been discretized with a grid size $\Delta\sigma/\langle\sigma\rangle = 0.02$, and truncated where $f(\sigma)\Delta\sigma \approx 10^{-8}$, i.e. at $\sigma_{\text{cut}}/\langle\sigma\rangle = 1.68$ and 3.48 , respectively. Since each diameter characterizes a different component, these discrete polydisperse mixtures involve $p = 85$ and 175 components. Note that these numbers of components are much larger than those used with the SHS-PY model of Ref. 20.

The effect of size polydispersity is considerable³⁷, as appears from a comparison among Figs. 1, 3a and 3b: with increasing s_σ at fixed η , $S_M(k)$ slightly increases in the low- k region,

its first peak is reduced and shifted to smaller k values, and all subsequent oscillations are progressively dumped, as a result of destructive interference among the several length scales involved.

3. SHS polydisperse in size but not in stickiness

At this point we study SHS fluids polydisperse in size but monodisperse in stickiness, with all particles having $Y_i = Y_{\langle\sigma\rangle} = \gamma_0 \langle\sigma\rangle$ ($s_\sigma \neq 0$, $\alpha = 0 \Rightarrow s_Y = 0$). This choice will be referred to as Model I and has been prompted by the SHS-PY investigations of Refs. 20-22, where a single, size-independent, stickiness parameter was considered.

Figures 4 and 5 illustrate what happens when a surface adhesion (with $\gamma_0 = 0.5, 0.7$) is added to size polydispersity. Comparison with Fig. 3 ($\gamma_0 = 0$) shows that the attractive interaction, in the presence of size polydispersity, produces a further lowering of oscillation amplitudes in the first peak region and beyond. When $\gamma_0 = 0.7$ and $s_\sigma = 0.3$ (Fig. 5b) all curves exhibit an almost complete flattening in the same range.

Near the origin (for $k \langle\sigma\rangle \lesssim 5$), for both considered cases with $\gamma_0 = 0.5$ (weak-attraction), only a small increase in $S_M(k)$ is found with respect to polydisperse HS without stickiness (Fig. 3), the relative ordering of all curves is unchanged and also coincides with that of the corresponding monodisperse SHS (Fig. 2a). On the other hand, when $\gamma_0 = 0.7$ and $s_\sigma = 0.1$ (strong-attraction and low size polydispersity, Fig. 5a) the behaviour of $S_M(k)$ close to the origin strongly differs from that of polydisperse HS without stickiness and is similar to the monodisperse SHS case of Fig. 2b. Surface adhesion produces large $S_M(0)$ values, which are, however, smaller than the corresponding monodisperse ones. This means that, when $\gamma_0 \neq 0$, size polydispersity reduces $S_M(k)$ even near the origin (whereas, when $\gamma_0 = 0$, increasing s_σ at fixed η determines an increase of $S_M(0)$). This effect of size polydispersity, in the presence of attraction, is amplified when $\gamma_0 = 0.7$ and $s_\sigma = 0.3$ (strong-attraction and high size polydispersity, Fig. 5b). Now one observes an interesting return to a ‘‘HS-like ordering’’ of the curves in the low- k region, as in the case $\gamma_0 = 0.5$. This behaviour is peculiar of

Model I and will be absent in Model II to be presented in the next subsection.

4. SHS polydisperse both in size and in stickiness

Next we consider the case of stickiness correlated to the size, according to the linear law $Y_i = \gamma_0 \sigma_i$ ($\alpha = 1$, $s_Y = s_\sigma \neq 0$). This will be referred to as Model II.

The results for $\gamma_0 = 0.5$, shown in Fig. 6, are qualitatively similar to those of Model I (Fig. 4). When $s_Y = s_\sigma = 0.1$ the quantitative differences are very small. However, when $s_Y = s_\sigma = 0.3$ the $S_M(0)$ values lie more clearly above those of Fig. 4b.

For $\gamma_0 = 0.7$ (Fig. 7) the behaviour of $S_M(k)$ in the first peak region and beyond is essentially unchanged with respect to Model I, but near the origin differences are larger and significant. Here, when $s_Y = s_\sigma = 0.1$ the $S_M(k)$ curves are similar to those of Fig. 5a, with larger $S_M(0)$ values (very close to the corresponding monodisperse ones of Fig. 2b), but as $s_Y = s_\sigma = 0.3$ there is a qualitative as well as quantitative difference with respect to Model I (Fig. 5b). Indeed in the low- k region the $S_M(k)$ curves of Fig. 7b exhibit the same relative ordering present in the previous case with lower polydispersity (Fig. 7a) as well as in the corresponding fully monodisperse fluid (Fig. 2b). This persistence in a “strong-attraction regime” even at high size polydispersity constitutes the main difference between Model I and II. Such a feature can be probably related to the fact that the stickiness distribution of Model II is skewed towards large Y_i values completely absent in Model I, and this asymmetry implies, on average, stronger attractive forces.

Unfortunately, the behaviour of $S_M(0)$ in polydisperse models does not admit any simple thermodynamical interpretation. For mixtures, in fact, the average structure factor $S_M(k)$ depends on the form factors and $S_M(0)$ is no longer the normalized compressibility³. Nevertheless, we have been able to account for the aforesaid difference of “regimes” between Model I and II when $\gamma_0 = 0.7$ and $s_\sigma = 0.3$ in terms of a single parameter, which generalizes the Boyle temperature of the monodisperse SHS case.

5. Generalized Boyle temperature

The Boyle temperature of these polydisperse models can be found by deriving their second virial coefficient B_2 from the low-density expansion of $S_{\text{NN}}(0) = 1 - 2B_2\rho + \mathcal{O}(\rho^2)$. Likewise, to interpret the behaviour of $S_{\text{M}}(k)$ previously discussed, we start from the low-density expansion of $S_{\text{M}}(0)$. A straightforward calculation, employing the dyadic formalism of Sections II and III and not reported here, yields

$$\widehat{Q}_{ij}^{-1}(0) = \delta_{ij} - \rho(x_i x_j)^{1/2} \left[\frac{\pi}{6} (\sigma_j^3 + 3\sigma_i \sigma_j^2) - 2\pi Y_i Y_j \sigma_j \right] + \mathcal{O}(\rho^2), \quad (49)$$

and therefore, from Eq. (12),

$$S_{ij}(0) = \delta_{ij} - \rho(x_i x_j)^{1/2} \left[\frac{\pi}{6} (\sigma_i + \sigma_j)^3 - 2\pi (Y_i Y_j \sigma_j + Y_j Y_i \sigma_i) \right] + \mathcal{O}(\rho^2). \quad (50)$$

Inserting this result into $S_{\text{M}}(0) = \sum_{i,j} (x_i x_j)^{1/2} [F_i(0) F_j^*(0) / P(0)] S_{ij}(0)$, and using the above mentioned expression for $F_m(k)$, we obtain $S_{\text{M}}(0) = 1 - 2B_{2,\text{F}}\rho + \mathcal{O}(\rho^2)$, with

$$B_{2,\text{F}} = \frac{\pi}{6} \frac{1}{\langle \sigma^6 \rangle} [\langle \sigma^6 \rangle \langle \sigma^3 \rangle + 3 \langle \sigma^5 \rangle \langle \sigma^4 \rangle - 12 \langle \sigma^3 Y \rangle \langle \sigma^4 Y \rangle], \quad (51)$$

which is the analogue of the second virial coefficient, including all form factors. The sign of $B_{2,\text{F}}$, and therefore the behaviour of $S_{\text{M}}(0)$ at low density (as well as the overall “regime” of $S_{\text{M}}(k)$), depends on T^* , which is hidden in the Y terms. On defining a *generalized Boyle temperature* $T_{\text{B,F}}^*$ as the one where $B_{2,\text{F}}$ vanishes, and employing our assumption $Y_i = \gamma_0 \sigma_i^\alpha / \langle \sigma \rangle^{\alpha-1}$, we find

$$T_{\text{B,F}}^* = \frac{12 \langle \sigma^{3+\alpha} \rangle \langle \sigma^{4+\alpha} \rangle}{[\langle \sigma^6 \rangle \langle \sigma^3 \rangle + 3 \langle \sigma^5 \rangle \langle \sigma^4 \rangle] \langle \sigma \rangle^{2(\alpha-1)}}. \quad (52)$$

Exploiting Eq. (40), it follows that

$$\begin{aligned} T_{\text{B,F}}^* &= 12 / [M_4 (M_5 + 3M_3)] \quad \text{for Model I,} \\ T_{\text{B,F}}^* &= 12M_3 / (M_5 + 3M_3) \quad \text{for Model II,} \end{aligned} \quad (53)$$

where M_j has been defined with reference to Eq. (40). The role of $T_{\text{B,F}}^*$ for $S_{\text{M}}(k)$ is the same as that of T_{B}^* for $S_{\text{mono}}(k)$ of monodisperse SHS: above $T_{\text{B,F}}^*$ the behaviour is “HS-like”, whereas a “strong-attraction regime” is found when $T_{\text{c}}^* < T^* < T_{\text{B,F}}^*$.

Eqs. (53) imply that, in both models, $T_{\text{B,F}}^*$ depends on the degree of size polydispersity s_σ . However, whereas $T_{\text{B,F}}^*(s_\sigma)$ of Model I is a rapidly decreasing function, in Model II it exhibits only a very slow decrease asymptotically approaching $18/7 \simeq 2.57$. Such a difference explains the behaviours displayed in Fig. 5 and 7, which refer to $T^* = 2.04$ (i.e. $\gamma_0 = 0.7$). In Model I, when $s_\sigma = 0.1$ one has $T^* < T_{\text{B,F}}^* = 2.79$, whereas when $s_\sigma = 0.3$ one finds $T^* > T_{\text{B,F}}^* = 1.68$. On the other hand, in both cases the temperature of Model II is below the generalized Boyle one, the values of $T_{\text{B,F}}^*$ now being 2.99 and 2.90 for $s_\sigma = 0.1$ and 0.3, respectively.

Finally, it is instructive to compare $T_{\text{B,F}}^*$ with the true Boyle temperature T_{B}^* of these polydisperse models. The second virial coefficient, obtained from the low-density expansion of $S_{\text{NN}}(0)$, turns out to be $B_2 = (\pi/6) [\langle \sigma^3 \rangle + 3 \langle \sigma^2 \rangle \langle \sigma \rangle - 12 \langle Y \rangle \langle \sigma Y \rangle]$, and one obtains $T_{\text{B}}^* = 12 / [M_1 (M_2 + 3)]$ and $12 / (M_2 + 3)$ for Model I and II, respectively. Note that for these polydisperse fluids it is always $T_{\text{B}}^* < (T_{\text{B}}^*)_{\text{mono}} = 3$, $T_{\text{B,F}}^* < T_{\text{B}}^*$ for Model I, and $T_{\text{B,F}}^* > T_{\text{B}}^*$ for Model II, while in the limit of monodisperse fluids $T_{\text{B,F}}^* \rightarrow (T_{\text{B}}^*)_{\text{mono}}$.

V. SUMMARY AND CONCLUSIONS

In this paper we have presented a new analytically solvable model for multi-component SHS fluids within the MSA closure, using a hard-core-Yukawa potential with factorizable coupling parameters (in the appropriate infinite amplitude and zero range limit). The model is simpler than previous ones available in the literature, since $\hat{q}_{ij}(k)$ is in general 3-dyadic (Tutschka and Kahl's model²⁷ was 5-dyadic), with a consequent great simplification of all analytical formulas.

We have stressed the importance of the ‘‘dyadic structure’’ of $\hat{q}_{ij}(k)$ and recalled the properties of matrices with dyadic elements. Such a feature allows the analytic inversion of $\hat{Q}_{ij}(k)$ required to get the partial structure factors $S_{ij}(k)$. Through Vrij's summation, expressions have then been obtained for global structure functions, such as $R(k)$, $S_{\text{M}}(k)$ and $S_{\text{NN}}(k)$. These closed analytical formulas, just as their counterparts for polydisperse HS¹³

and CHS⁸, allow to “bypass” the computation of the individual $p(p + 1)/2$ partial structure factors, which may be a rather difficult task for polydisperse systems with large number of components. Because of their simplicity, our expressions may therefore represent a very useful tool to fit experimental scattering data of real colloidal fluids.

While the presented 3-dyadic expressions hold true for any choice of stickiness parameters Y_i , two particular versions of the model have been analyzed numerically. The first one assumes size polydispersity, but a single stickiness parameter for all particles (Model I), while the second one proposes stickiness parameters dependent on the diameters according to a linear law (Model II). Model I is similar to the SHS-PY models for polydisperse colloids known in the literature^{20–22}, while Model II is the simplest choice for size-dependent stickiness parameters.

The combined influence of hard core repulsion, adhesive attraction and polydispersity can generate a variety of behaviours at the level of measurable average structure factor $S_M(k)$. We have recognized the existence of two different “regimes” for $S_M(k)$ both in monodisperse and in polydisperse SHS fluids. Above a temperature $T_{B,F}^*$, which in the monodisperse case coincides with the Boyle temperature, we have identified a “weak-attraction” behaviour, resembling the HS one. In the range below $T_{B,F}^*$ but still above the critical temperature, a “strong-attraction” regime sets in, and we have described its features in detail. It is found that $T_{B,F}^*$ is a decreasing function of the degree of size polydispersity s_σ . It is also worth noting that the behaviour of our SHS-MSA models in the “strong-attraction regime” is in qualitative agreement with that of the SHS-PY model displayed in Figs 3 and 4 of Ref. 20, where the existence of two different “regimes” for $S_M(k)$ was, however, not recognized.

All our numerical results show that size polydispersity strongly affects the behaviour of $S_M(k)$ in the first peak region and beyond, where the influence of stickiness polydispersity is less significant. Models I and II are nearly equivalent in this interval of k -values, whereas they may substantially differ near the origin. The present study shows that the use of a single stickiness parameter, instead of more realistic size-dependent ones, may lead to marked differences in the small angle scattering region at sufficiently high γ_0 , i.e. when

attraction is strong or temperature is low.

In the small k region the adhesive forces and the specific relationship between stickiness and size parameters have far reaching consequences. Although very little is known experimentally about the correlation between stickiness and size, it is reasonable to expect that larger particles attract each other more strongly. The linear dependence $Y_i = \gamma_0 \sigma_i$ represents the simplest non-trivial choice, but other possibilities could also be taken into account²⁷. Duits *et al.*²² found that in some cases the SHS-PY model with a single stickiness parameter, independent of particle size, was unable to fit their experimental scattering data, and these authors already emphasized the possible role of stickiness polydispersity as a cause for the observed deviations. Similar discrepancies between experimental and model $S_M(k)$ values could be a crucial test for the soundness of our Model II with respect to Model I, as well as of any other choice for the stickiness-size functional relationship.

It would be also instructive to compare our SHS-MSA model with other recent theoretical approaches to polydisperse colloidal fluids. As an example, we mention the “optimized random phase approximation” joined with orthogonal polynomial expansions, proposed by Lado and coworkers⁴¹.

However, the most important advantage of the present model lies in its simplicity. In particular, version II has special formal properties, since - only in this case - the expression of $\widehat{q}_{ij}(k)$ becomes 2-dyadic. Therefore version II can indeed be reckoned as the simplest solvable model for polydisperse SHS and it could be a good candidate to tackle the issue of thermodynamics and phase stability of these fluids from a fully analytical point of view. We expect that compact expressions for pressure, chemical potentials, partial structure factors at $k = 0$, as well as other quantities required to investigate - for instance - sedimentation⁴², vapor-liquid equilibrium and demixing in the presence of polydispersity, can easily be obtained. We hope to accomplish this task in a forthcoming paper.

ACKNOWLEDGMENTS

Partial financial support by the Italian MURST (Ministero dell'Università e della Ricerca Scientifica through the INFN (Istituto Nazionale di Fisica della Materia) is gratefully acknowledged.

FIGURES

FIG. 1. PY (\equiv MSA) structure factor S_{mono} of monodisperse hard spheres without stickiness, plotted as a function of the dimensionless variable $k\sigma$ at various packing fractions η . Note that this and all following figures have the same scale.

FIG. 2. MSA structure factor S_{mono} of monodisperse sticky hard spheres, plotted as a function of $k\sigma$ at various packing fractions η , for two values of adhesive strength parameter γ_0 (here, and in all following figures, the curves of Part b) are shifted upwards by 2.5 units).

FIG. 3. PY (\equiv MSA) structure factor S_M of polydisperse hard spheres without stickiness, plotted as a function of $k\langle\sigma\rangle$ at various packing fractions η , for two different degrees of size polydispersity s_σ .

FIG. 4. MSA structure factor S_M of sticky hard spheres polydisperse in size but monodisperse in stickiness (Model I), plotted as a function of $k\langle\sigma\rangle$ at various packing fractions η , for $\gamma_0 = 0.5$ and two different degrees of size polydispersity s_σ .

FIG. 5. As Fig. 4 but for $\gamma_0 = 0.7$.

FIG. 6. MSA structure factor S_M of sticky hard spheres polydisperse in size and stickiness (Model II), plotted as a function of $k\langle\sigma\rangle$ at various packing fractions η , for $\gamma_0 = 0.5$ and two different degrees of size polydispersity s_σ .

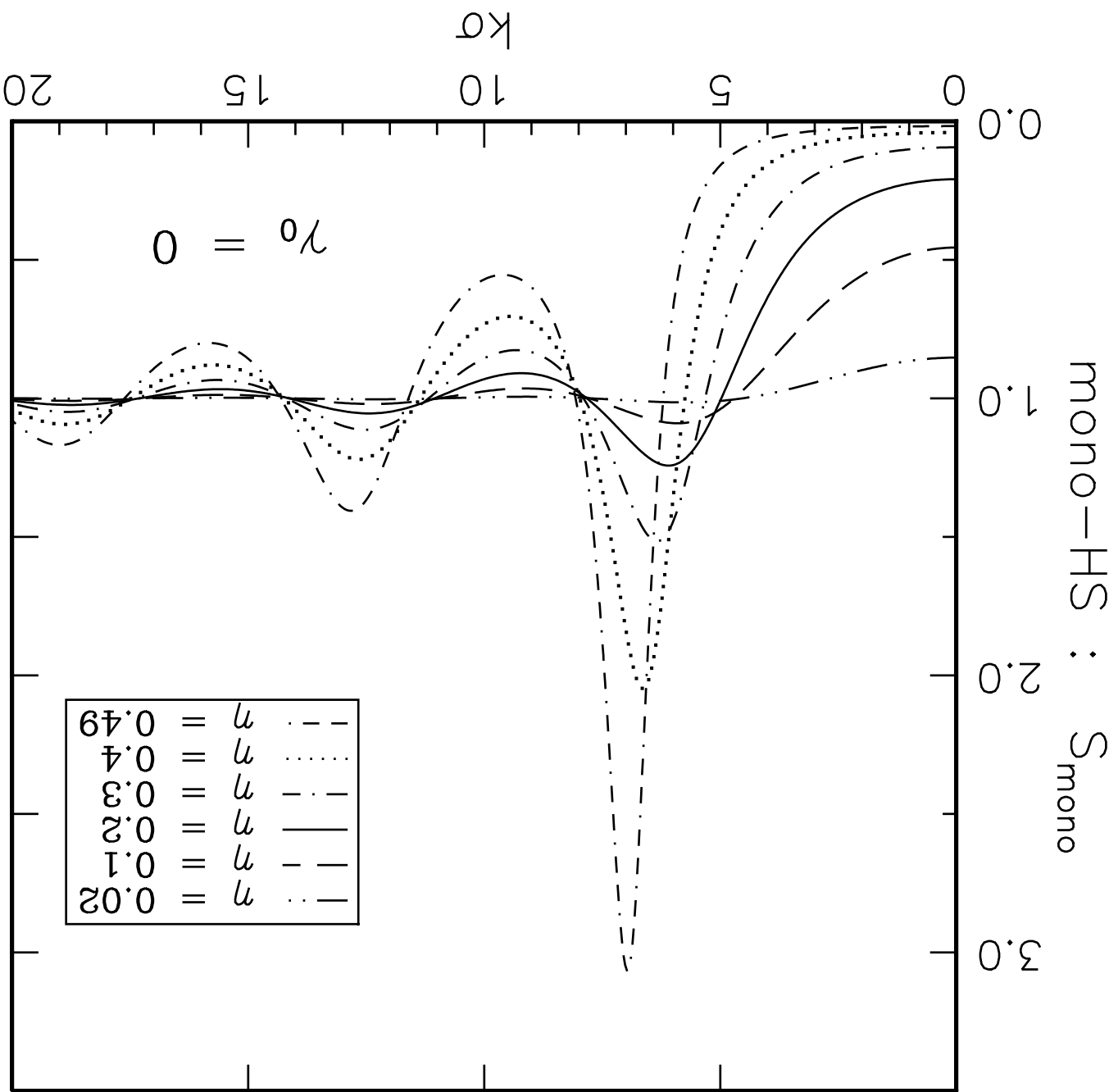
FIG. 7. As Fig. 6 but for $\gamma_0 = 0.7$.

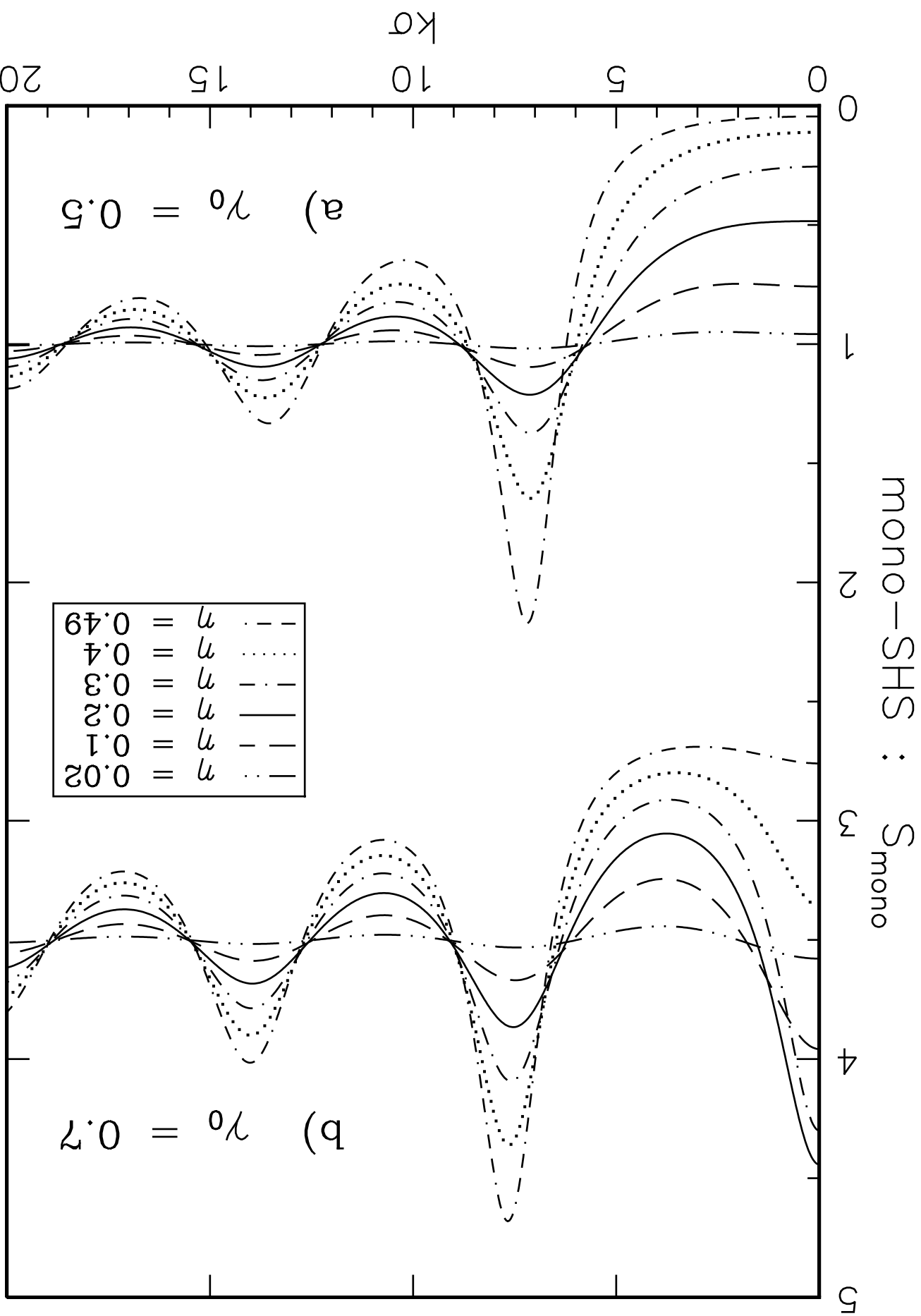
REFERENCES

- ¹ P. N. Pusey in: *Liquids Freezing and Glass Transition: II, Les Houches Sessions 1989*, eds. J. P. Hansen, D. Levesque and J. Zinn-Justin (North-Holland, Amsterdam, 1991) pp. 763-942.
- ² H. Löwen, Phys. Rep. **249**, 5 (1994).
- ³ G. Nägele, Phys. Rep. **272**, 215 (1996).
- ⁴ L. Blum and G. Stell, J. Chem. Phys. **71**, 42 (1979); *ibidem*, (Erratum) **72**, 2212 (1980).
- ⁵ J. P. Hansen and I. R. Mc Donald *The Theory of Simple Liquids* (Academic, London) (1986).
- ⁶ R. J. Baxter, J. Chem. Phys. **52**, 4559 (1970).
- ⁷ K. Hiroike, Prog. Theor. Phys. **62**, 91 (1979).
- ⁸ D. Gazzillo, A. Giacometti and F. Carsughi, J. Chem. Phys. **107**, 10141 (1997).
- ⁹ N. W. Ashcroft and D. C. Langreth, Phys. Rev. **156**, 685 (1967).
- ¹⁰ W. L. Griffith, R. Triolo and A. Compere, Phys. Rev. A **33**, 2197 (1986).
- ¹¹ G. Senatore and L. Blum, J. Phys. Chem. **89**, 2676 (1985).
- ¹² M. Ginoza and M. Yasutomi, Phys. Rev. E **59**, 2060 (1999).
- ¹³ A. Vrij, J. Chem. Phys. **69**, 1742 (1978); *ibidem* **71**, 3267 (1979).
- ¹⁴ R. J. Baxter, J. Chem. Phys. **49**, 2270 (1968).
- ¹⁵ G. Stell, J. Stat. Phys. **63**, 1203 (1991).
- ¹⁶ C. Regnaut and J. C. Ravey, J. Chem. Phys. **91**, 1211 (1989).
- ¹⁷ J. W. Perram and E. R. Smith, Chem. Phys. Lett. **35**, 138 (1975).
- ¹⁸ B. Barboy and R. Tenne, Chem. Phys. **38**, 369 (1979).

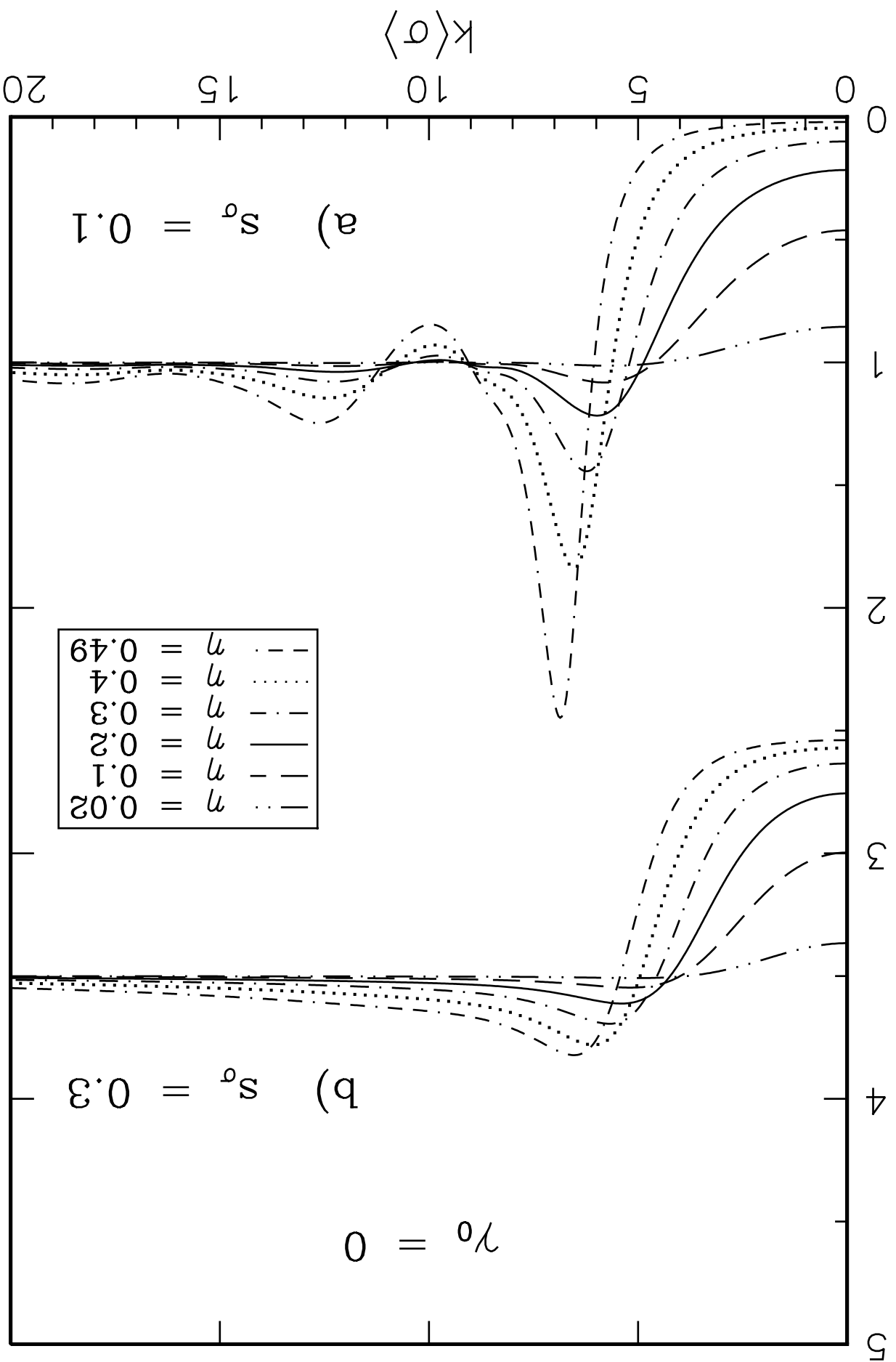
- ¹⁹ A. Santos, S. B. Yuste and M. López de Haro, J. Chem. Phys. **109**, 6814 (1998).
- ²⁰ C. Robertus, W. H. Philipse, J. G. H. Joosten and Y. K. Levine, J. Chem. Phys. **90**, 4482 (1989).
- ²¹ M. H. G. M. Penders and A. Vrij, J. Chem. Phys. **93**, 3704 (1990).
- ²² M. H. G. Duits, R. P. May, A. Vrij, and C. G. de Kruif, Langmuir **7**, 62 (1991).
- ²³ J. N. Herrera and L. Blum, J. Chem. Phys. **94**, 6190 (1991).
- ²⁴ J. J. Brey, A. Santos and F. Castano, Mol. Phys. **60**, 113 (1987).
- ²⁵ L. Mier-y-Teran, E. Corvera and A. E. Gonzalez, Phys. Rev. A **39**, 371 (1989).
- ²⁶ M. Ginoza and M. Yasutomi, Mol. Phys. **87**, 593 (1996).
- ²⁷ C. Tutschka and G. Kahl, J. Chem. Phys. **108**, 9498 (1998).
- ²⁸ A. B. Bhatia and D. E. Thornton, Phys. Rev. **B2**, 3004 (1970).
- ²⁹ L. L. Lee, *Molecular Thermodynamics of Nonideal Fluids* (Butterworths, Boston, 1988).
- ³⁰ J. Mathews and R. L. Walker, *Mathematical Methods of Physics* (Benjamin, NY 1965).
- ³¹ L. Blum and J. S. Høye, J. Phys. Chem. **81**, 1311 (1977).
- ³² L. Blum and J. S. Høye, J. Stat. Phys. **14**, 317 (1978).
- ³³ M. Yasutomi and M. Ginoza, Mol. Phys. **89**, 1755 (1996).
- ³⁴ J. N. Herrera, L. Blum and P. T. Cummings, Mol. Phys. **98**, 73 (1998).
- ³⁵ D. Gazzillo, A. Giacometti, R. G. Della Valle, E. Venuti and F. Carsughi, J. Chem. Phys. **111**, 7636 (1999).
- ³⁶ D. Gazzillo, A. Giacometti, and F. Carsughi, Phys. Rev. E **60**, 6722 (1999).
- ³⁷ P. van Beurten and A. Vrij, J. Chem. Phys. **74**, 2744 (1981).

- ³⁸ B. D'Aguzzo and R. Klein, *J. Chem. Soc. Faraday Trans.*, **87**, 379 (1991).
- ³⁹ M. Abramowitz and I.A. Stegun, *Handbook of Mathematical Functions* (Dover, New York, 1972).
- ⁴⁰ N. H. March and M. P. Tosi, *Atomic Dynamics in Liquids* (MacMillan, London, 1976).
- ⁴¹ S. Leroch, G. Kahl and F. Lado, *Phys. Rev. E* **54**, 6937 (1999).
- ⁴² P. G. Bolhuis and H. N. W. Lekkerkerker, *Physica A* **196**, 375 (1993).

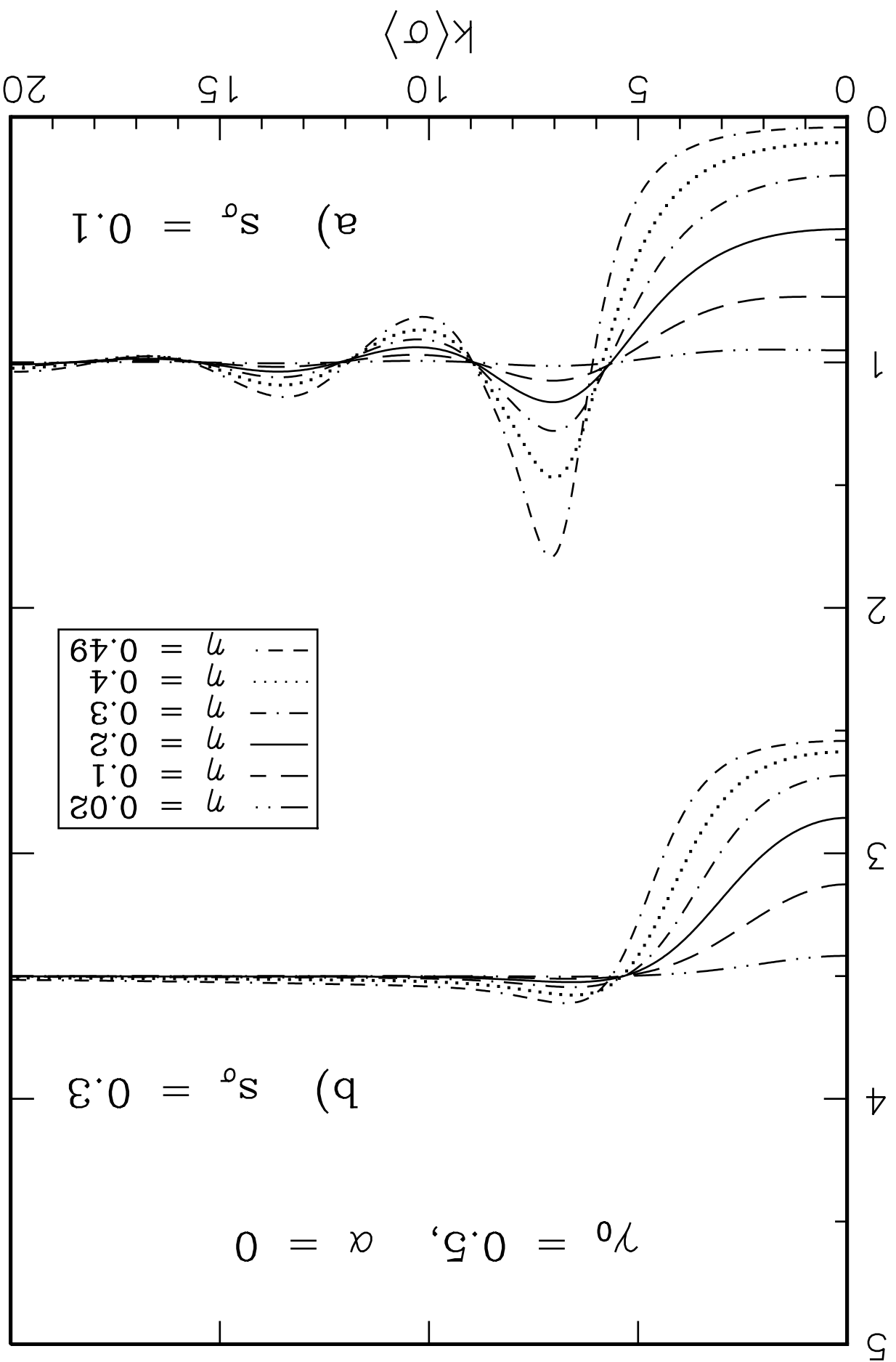




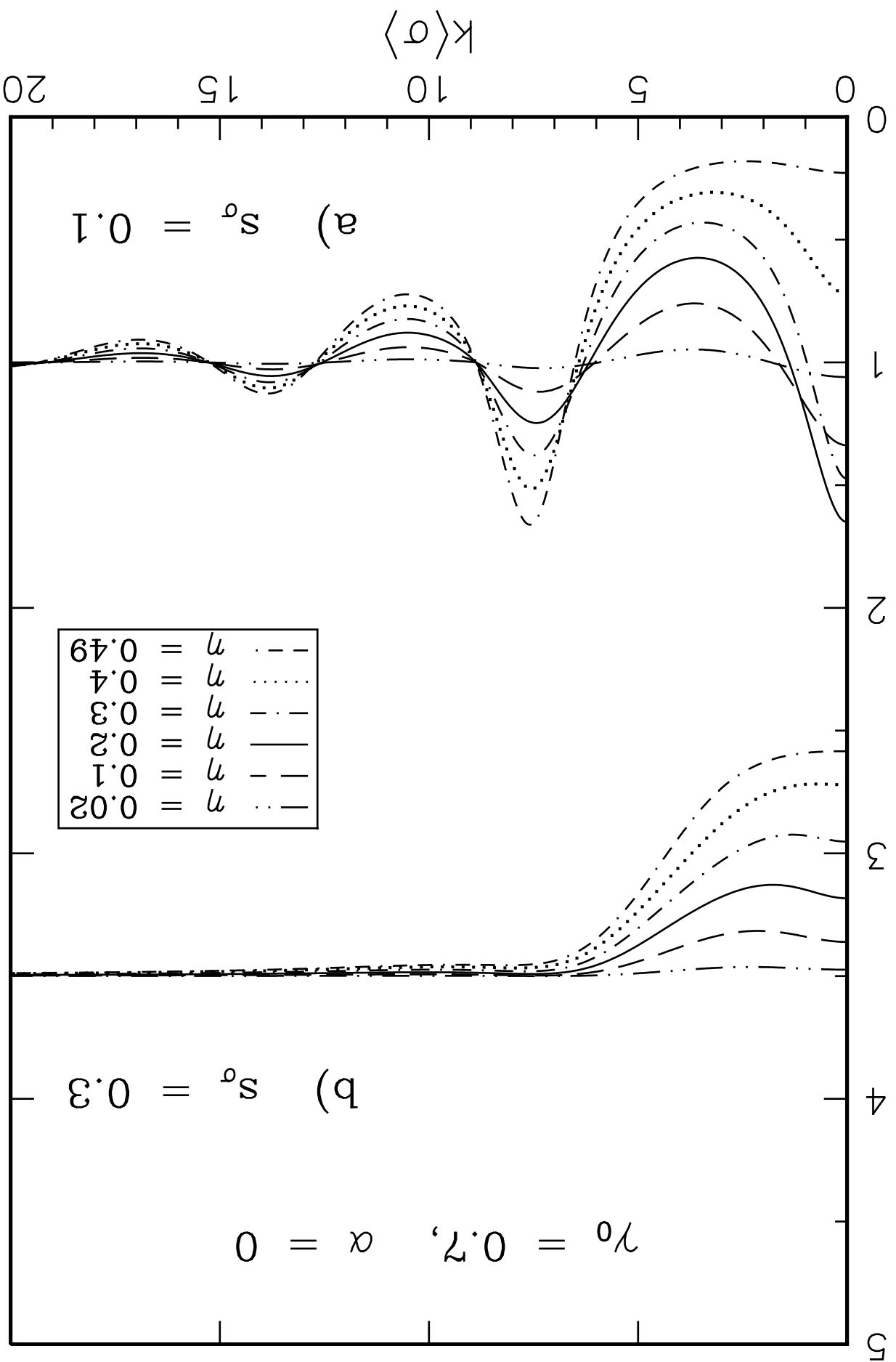
poly-HS : S_M



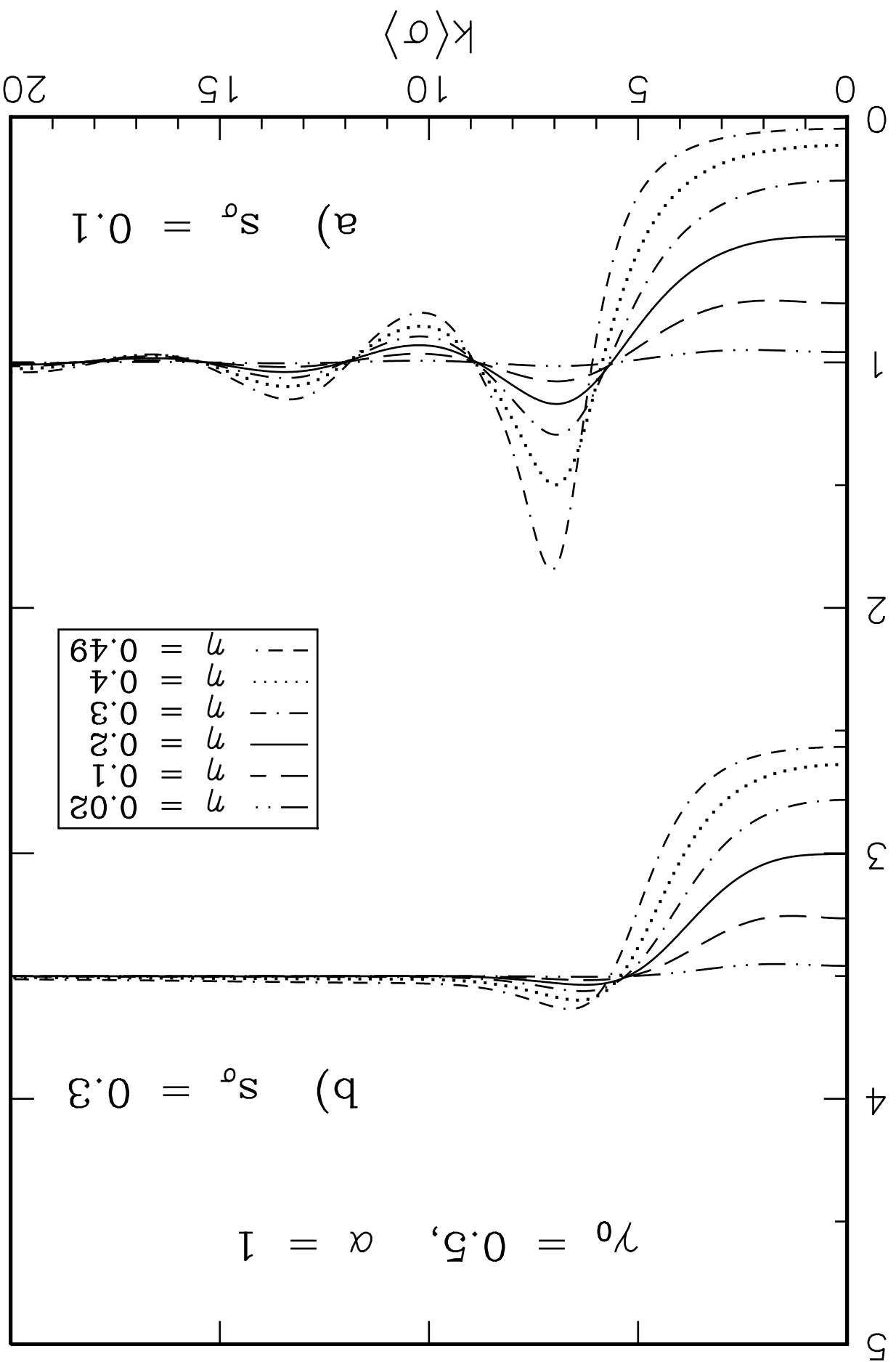
poly-SHS : S_M



poly-SHS : S_M



poly-SHS : S_M



poly-SHS : S_M

